Stability of Self-Standing High Stiffness-Steel Pipe Sheet Pile Walls Embedded in Soft Rocks

Vijayakanthan KUNASEGARAM
PhD Student, Dept. of Civil and Environmental Engineering, Tokyo Institute of Technology, Tokyo, Japan
Email: vijayakanthan.k.aa@m.titech.ac.jp, heshuvijay@gmail.com
Jiro TAKEMURA
Associate Professor, Dept. of Civil and Environmental Engineering, Tokyo Institute of Technology, Tokyo, Japan
Yoshiro ISHIHAMA
Senior Researcher, Steel Structures Research Lab, Nippon Steel and Sumitomo metal Corporation, Chiba, Japan
Yukihiro ISHIHARA
Manager, Press-in Technologies Support Department, IPA Support Section, GIKEN LTD, Tokyo, Japan

ABSTRACT

Five centrifuge model tests are reported in this paper, which discusses the overall behaviours of self-standing stiff sheet pile walls embedded in soft rocks. Two different soft rocks, namely sand rock and mud rock were modelled by using sand-cement-clay mixtures at appropriate mixing ratios. In this study, a centrifuge modelling technique has been developed in which the loading process can be simulated from design conditions to the ultimate failure conditions on an embedded wall in soft rock. A series of centrifuge tests has been carried out to investigate the influence of embedment depth on the stability of self-standing steel pipe sheet pile walls. Experimental observations reveal that, the stiff sheet pile walls suffer from rigid body rotations about a pivot point. An equilibrium analysis was performed by switching the active and passive zones based on the observed pivot point at the verge of rotational failure. A similar contribution of increment in embedment depth on the stability of walls can be confirmed from the analysis and experimental outcomes. Also, it can be confirmed that the wall can stand in the design condition with a reasonable safety margin with a relatively small embedment depth compared to current design practices and a small increment in embedment depth e.g., 0.5m, can significantly increase the wall stability and prevent the wall from ultimate collapse.

Key words: *Self-standing walls, Soft rock, Stability, Centrifuge model, Steel pipe piles*

1. Introduction

Urban development with existing infrastructures often encounters certain physical restrictions for the application of earth retaining structures. In such situations due to simple retaining mechanism and applicability under limited space, self-standing walls could be an ultimate choice of an engineer. Large diameter steel pipe piles can be effectively utilized for a self–standing sheet pile wall with a relatively large retained height. Deflection of the wall below the allowable limit and the flexural bending failure can be prevented due to the high flexural stiffness and strength of large diameter piles. However, for the application of large diameter piles as a self-standing wall, relatively large stiffness and strength are required for the embedment ground, such as dense sand or soft rock to secure the passive resistance against the lateral and moment loads from the retained soils. The current design practice in Japan requires a minimum embedment depth for a self-standing sheet pile wall. In the design method, based on the characteristic value β obtained by Chang's equation, the minimum embedment depth of $(2.5–3)/\beta$ is being used as described in the design manual of self-standing steel sheet pile wall (2009). Referring to this method, the requirement of minimum embedment depth increases with the increasing EI value, which causes difficulties in the installation of large diameter piles into the hard ground such as soft rock and eliminates the applicability of large diameter piles. Therefore, if this type of retaining wall can be constructed with a relatively small embedment depth in soft rock type ground, its applicability can be increased, which would contribute to the reduction of construction time and cost. For the reduction of embedment depth smaller than the one determined by the current design practice, both serviceability and ultimate limits should be reasonably examined in the design with an additional margin of safety.

2. Centrifuge modelling

Centrifuge model studies were conducted using TIT Mark III geotechnical centrifuge at 50g centrifugal acceleration, the specifications of centrifuge facility are listed in Takemura et al. (1999). An illustration of a centrifuge model arrangement is given in **Fig. 1**, which represents a self-standing sheet pile wall embedded in artificially made soft rock. In the centrifuge model, a model wall was placed throughout the breadth of the container to secure the plane strain deformations of the wall. Soft rock model was prepared in a container which had the internal dimensions of 700 mm in length, 150 mm in breadth and 500 mm in depth. The container was made up of a removable steel frame on the rear face and a transparent acrylic panel stiffened by a steel hollow frame in the front; both face panels were bolted with the frame in the front; both face panels were bolted with the main body to form a rigid container. Two box-shape rubber bags were placed on the front and back sides of the wall. The front one was a polypropylene-made closed box with pile at the bottom corner and the top of the box was filled with water. The back side one was an open box made of latex rubber, which was filled with dry sand. Detailed modelling procedures about the centrifuge model are described in Kunasegaram et al. (2018).

2.1. Test conditions and model sheet pile walls

This paper reports the results of five centrifuge model tests, which are divided into two test series, i.e., sand rock and mud rock series, as shown in **Table 1**. All dimensions and the properties of the model walls are given in prototype scale in **Table 1**. Model sheet pile walls were made up of aluminium (A5052-O) alloy plates having the yield strength of 95 MPa and the Young's modulus of 69 GPa. Rigid and flexible sheet pile walls having the thickness of 24.9 mm and 9.9 mm in model scale are illustrated **Fig. 2**. The transformed sections of rigid and flexible model sheet pile walls were designed to replicate the flexural rigidities of steel pipe sheet pile walls with the Diameter (Ø) of 2.5 m, thickness t=25 mm and Ø=1.0 m, t=10 mm respectively. **Fig. 3,** shows the dimensions of large diameter piles and corresponding transformed sections in prototype scale. Considering the currently available technology for the installation (Gyropress method) of large diameter piles, an 0.18 m gap between two piles is inevitable. Therefore, in the modelling of equivalent rectangular section, an effective width

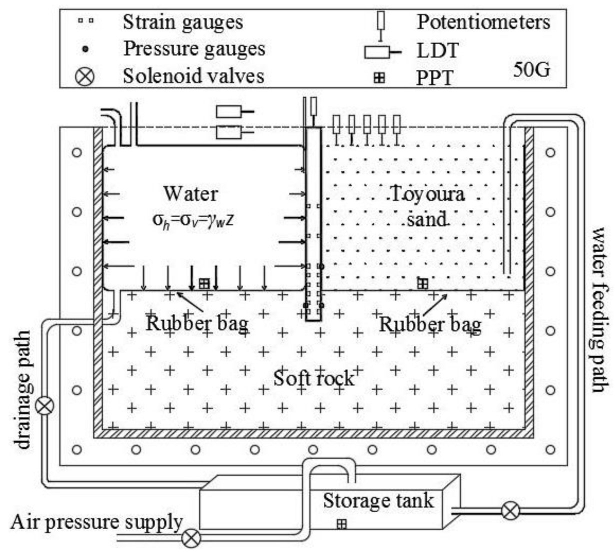

Fig. 1 Centrifuge model arrangement

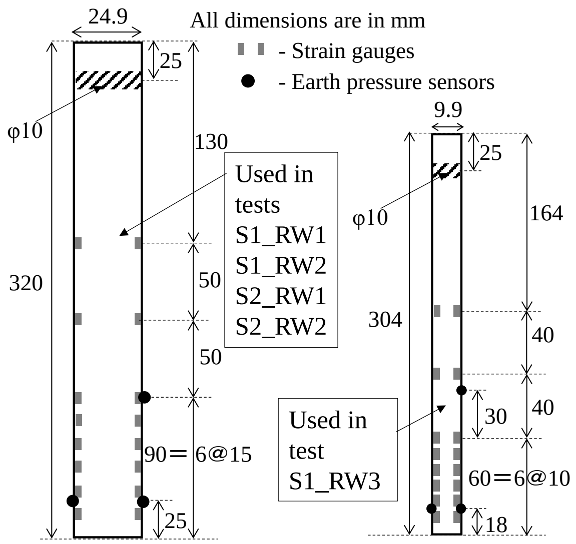

Fig. 2 Model Sheet pie walls used in experiment

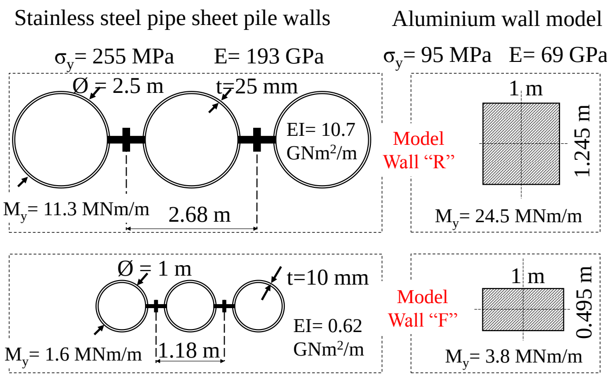

All dimensions are in prototype scale

Fig. 3 Transformed sections of wall "R" and wall "F"

Table 1. Test conditions

Test code	Rock type	Wall type	H (m)	d_e (m)	EI $_{wall}$ (GNm^2/m)
S1_RW1	Sand rock	R	12	2.5	11.096
S1_RW2		R	12	3.0	11.096
S1_RW3		F	9	1.8	0.697
S2_RW1	Mud rock	R	12	2.5	11.096
S2_RW2		R	12	3.0	11.096

H- Wall height d_e-Embedment depth

of 2.68 m and 1.18 m are considered for the wall 'R' and the wall 'F' respectively.

2.2. Properties of artificial soft-rock

Mechanical properties of artificial soft rocks were investigated through the unconfined compression (UC) tests which were conducted for the cylindrical molded specimens ($Ø$=50mm and L=100mm). The physical and mechanical properties of model soft rocks are presented in **Table 2**. In this study, the averaged external strain (dial gauge: ε_{ad}) and the surface strain (strain gauge: ε_{as}) of the specimens were measured by using a dial gauge and a pair of strain gauges, respectively. Secant modulus (E_{50}) of the artificially made rock samples were estimated based on the averaged external strain ($E_{50\_\varepsilon ad}$) and the averaged strain gauge ($E_{50\_\varepsilon as}$) measurements. The detailed procedures about soft rock modelling for centrifuge studies are described in Kunasegaram et al. (2015). Typical stress-strain behaviors of model soft rocks are illustrated in **Fig. 4**, along with the natural soft rocks encountered in Melbourne (Johnston, 1984) and Calgary

Table 2. Physical and mechanical properties of soft rocks

Embedment medium	Sand rock	Mud rock
Water/Cement ratio (%)	395	510
Water content (%)	21.5	39
Clay: Sand (wt. %)	30:70	100:0
Bulk density (kg/m^3)	2060	1820
Dry density (kg/m^3)	1715	1320
Unconfined Compressive Strength (UCS) (MPa)	1.3	1.0
$E_{50\_\varepsilon ad}$ - $E_{50\_\varepsilon as}$ (MPa)	260-660	200-420

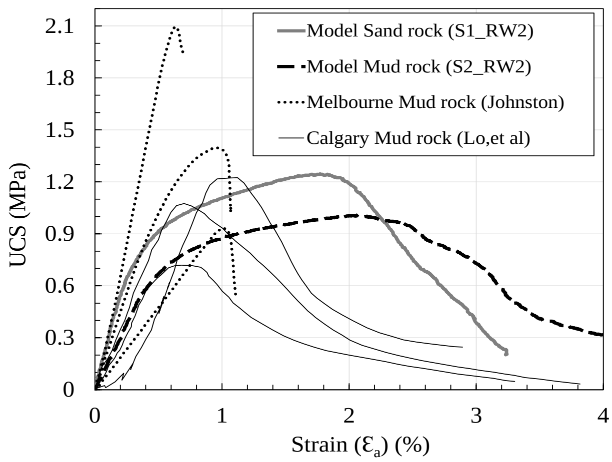

Fig. 4 Stress-strain behaviour of centrifuge model and natural soft rocks

(Lo, et al., 2009). From the stress strain behavior, up to 0.4% axial strain the model soft rocks exhibit similar However, the post peak behaviors of natural rocks are more brittle compared to the model rocks.

2.3. Simulation of Excavation and loading

The main objective of this modelling process was to simulate the excavation under serviceability limit states and achieving the ultimate failure conditions with the application of additional lateral loading under a constant centrifugal acceleration. Although the small deformation to large ultimate failures could be achieved by different alternative way such as increasing the centrifugal acceleration, such an alternative cannot predict the behavior of specific prototypes as the self-weight of the soil change with the centrifugal acceleration.

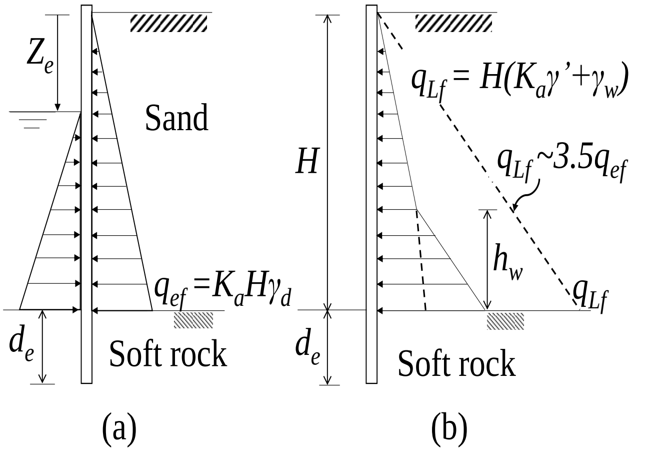

Fig. 5 Pressure distribution during (a) Excavation & (b) Loading

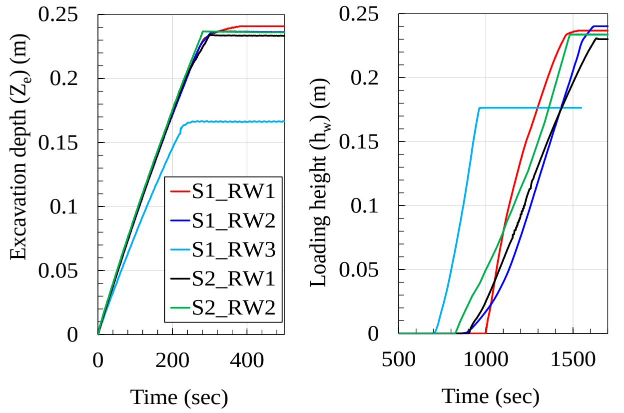

Fig. 6 Measured excavation depth and loading height in model scale

Therefore, it cannot be applied for the verification or design method.

In this study, unloading in the wall front and additional loading in the back side of the wall were achieved by using water as a draining and filling liquid respectively. The excavation process and the loading process after the excavation were simulated in a constant centrifugal acceleration as shown in **Fig. 5.** Referring to **Fig. 5** the excavation depth and the loading height of water in the back side of the wall are indicated by Z_e and h_w respectively. Also the notations q_{ef} and q_{Lf} represents the applied load intensities at the end of excavation and at the end of loading respectively.

Utilization of a heavy liquid having the identical unit weight of back fill material could create the vertical stress similar to that of the sand. However, the unbalance of horizontal stresses at the initial condition and the backward wall movements caused by the heavy liquid could be higher than those caused by water as a draining liquid. It is important to note that the earth pressure coefficient (K) in the retained soil is expected to be higher than the earth pressure coefficient at rest (K_0=1-sinϕ'$\sim$ 0.35), which can be attributed to the backward movement of the wall due to relatively larger water pressure than at rest earth pressure of the sand with γ_d=15.6 kN/m^3.

The unloading in the excavation process at the wall front was simulated by draining out the water from the rubber bag with the help of solenoid valves to the storage tank. After the excavation process, to create the ultimate loading condition, in other words to create large wall deflection, the additional load was applied by feeding the drained water in the tank to the backside rubber box, which was done by raising the air pressure of the tank manually. Due to the difficulty in monitoring and controlling the pressures, the variations of water height were different as shown in **Fig. 6.** The horizontal lateral pressure applied to the wall can be increased about 3.5 times the dry sand condition at the submerged state as described in **Fig. 5**. Excavation depths and the water heights in the two loading processes were measured by the pore pressure transducers placed at the bottom of both rubber bags.

3. Results and discussion

3.1. Observed behaviors

The way of increasing wall top displacements and rotations with the excavation depth and the additional lateral loading are shown in **Fig. 7** and **Fig. 8** respectively. Unlike a convex shape displacement and rotation profile with the increase of excavation depth in field, a concave shape behavior can be observed in all test cases. This phenomenon could be attributed to the utilization of fluid in the wall front which has the lateral earth pressure coefficient of unity and zero stiffness. Considering the difference between unloading by fluid and the real field excavations, in the case of real field excavation the mobilized passive earth pressure also increases with the lateral movement of wall, which could control the wall deflections at the initial stage of excavation with a larger supporting height of earth in the wall front. This phenomenon results in a convex shape load displacement behavior in real field excavation. However, it cannot be expected from a fluid with zero stiffness.

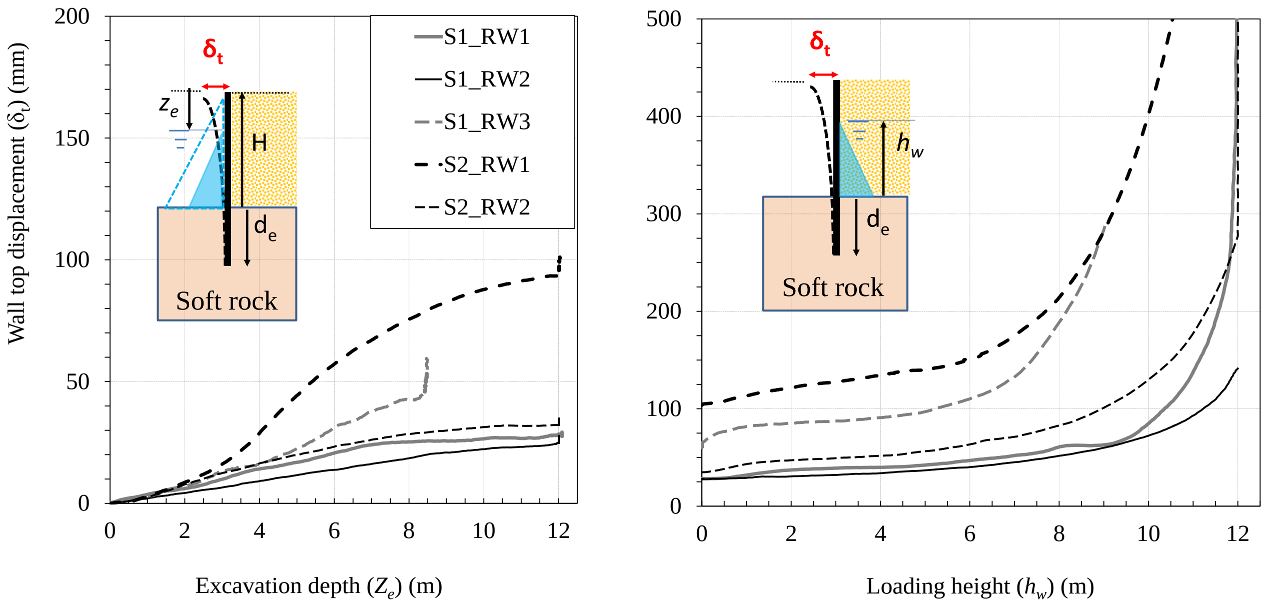

Fig. 7 Variation of measured wall top displacement with excavation depth and loading height

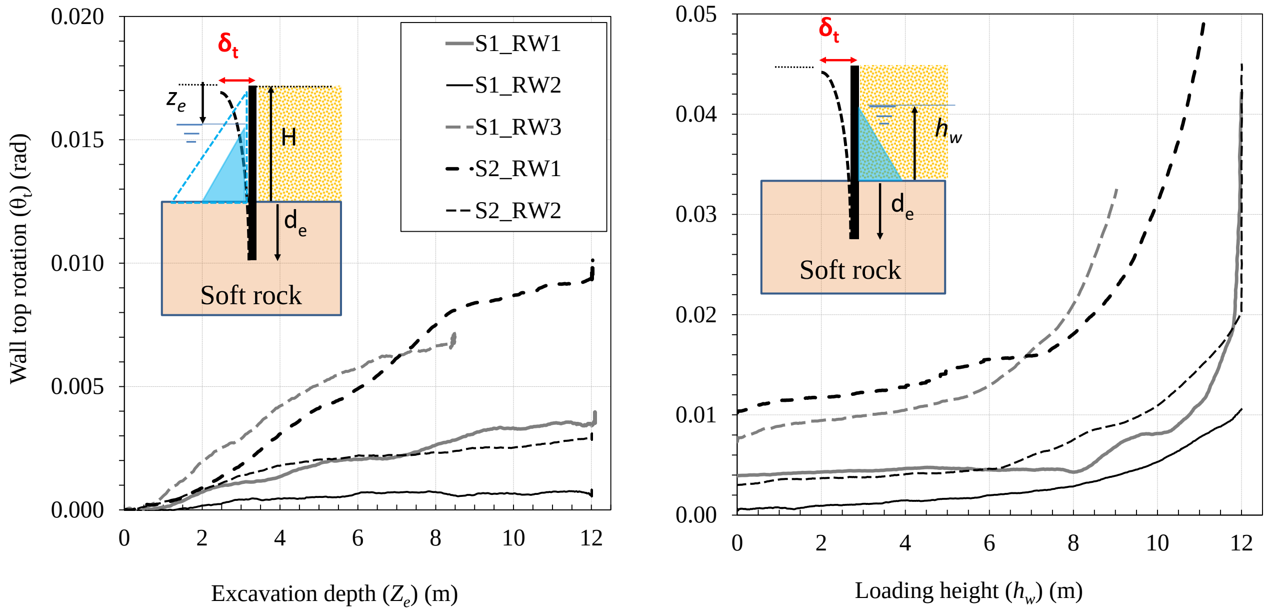

Fig. 8 Variation of wall top rotation with excavation depth and loading height

Considering the uncertainty in the initial condition of the modelling process in this study, a nonlinear variation of earth pressure coefficient with the excavation depth was selected in which the K value at initial condition is equal to $0.63(\gamma_w/\gamma_d)$ and decreasing non-linearly to achieve K_a at the end of excavation. However, during the loading process, $K=K_a$ was used to estimate the moment loads with the assumption of full mobilization of active earth pressures, where K=0.63 is the calculated K value to maintain the equilibrium with water pressure, and K_a is the active earth pressure coefficient of sand. Calculated moment loads for constant and non-linear K values are presented in **Fig. 9** against the excavation depth and loading height.

Fig. 10 shows the variation of normalized wall top displacements against the estimated moment loads at the dredge level. From **Fig. 10,** a similar increasing trend of displacements against the moment load with different system stiffness can be observed. Considering the resistance against moment loads or stiffness of observed

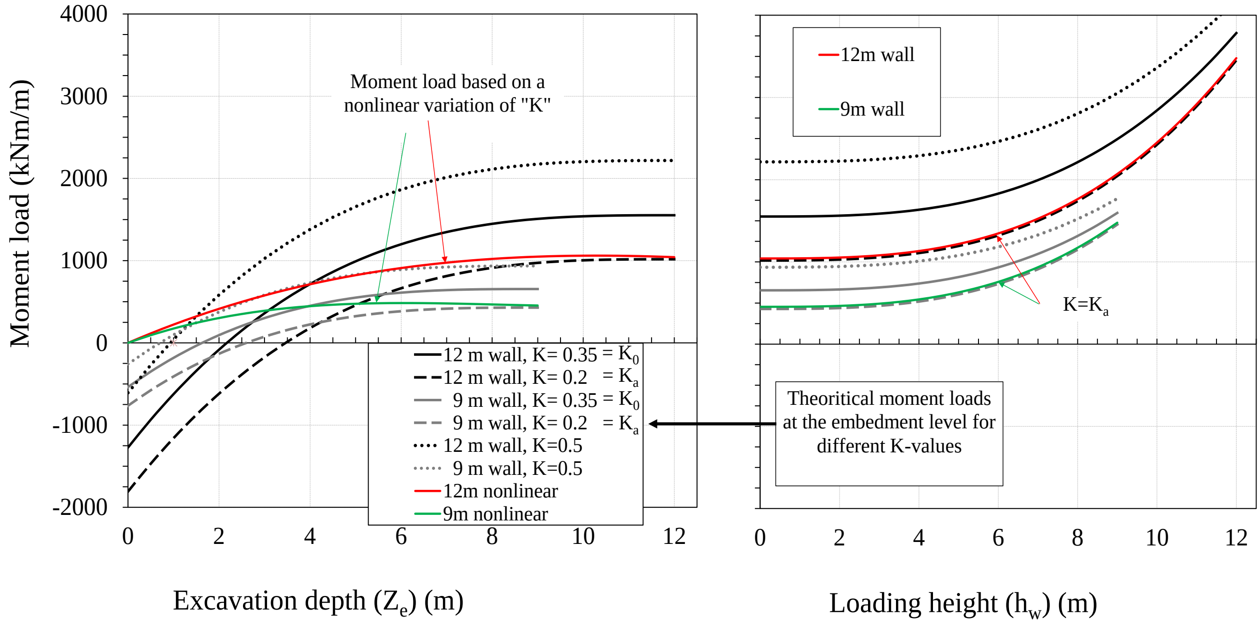

Fig. 9 Variation of theoretical moment loads at dredge level with excavation depth and loading height

curves, the wall in S1_RW3 exhibits large plastic deformations under small increment of moment loads. Although the ratio of the wall height to the embedment depth (H/d_e=5) is almost similar to that of the walls in S1_RW1 and S2_RW1 (H/d_e=4.8), observed large deformations at small load levels could be attributed to relatively small flexural stiffness of the wall. This observation clearly indicates the necessity of walls with high flexural stiffness to sustain large bending moments.

Considering the similar embedment and loading conditions of walls embedded in sand and mud rocks (S1_RW1, S2_RW1 and S1_RW2, S2_RW2), walls in mud rock exhibit large displacements and rotations compared to the ones in sand rock. Difference in the behaviors is as expected, since the model sand rock poses higher initial stiffness compared to the mud rock as shown in **Fig. 4**. From the physical observations given in **Fig. 11** and observed moment load displacement behaviors at the end of loading process, clear failures of the walls can be observed except the case of S1_RW2. The observation clearly indicates that, the stability of self-standing walls embedded in hard mediums can be maintained with relatively small embedment depth (d_e=3m) than that of the current design practice.

Referring to the observed stiffness of moment load displacement relation to the walls embedded in mud rock (S2_RW1 & S2RW2), a significant contribution of 0.5 m increment in embedment depth can be seen from small to large wall top displacements. However, there is no significant difference that can be seen for the walls embedded in sand rock up to 60 mm (0.5%*H*) wall top displacement. Up on initiation of yield deformation around 60 mm wall top displacement, the wall in S1_RW1 undergoes large plastic deformation and exhibits the collapse of the wall under a constant applied load. A similar behavior can be observed upon yielding at different wall top displacements for the cases S1_RW3, S2_RW1 & S2_RW2. However, the wall in S1_RW2 exhibits high resistance even at large moment loads compared to the other cases. At the end of loading process, the stability of the wall was confirmed with an induced wall top displacement of 185mm (1.5%*H*). Comparing this observation with the case of S1_RW1, a significant contribution of 0.5 m increment in embedment depth on the stability and failure behavior of self-standing walls can be confirmed.

Up on completion of loading process in order to create the failure of wall in S1_RW2, the centrifugal acceleration was gradually increased up to 95g as described in **Fig.10**. Although a gradual increase of displacement could be observed with the increase of acceleration, there is no clear failure of the embedded

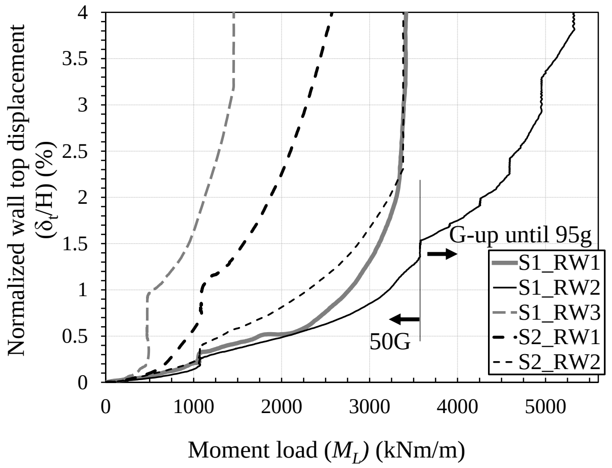

Fig. 10 Variation of normalized wall top displacement with applied moment load at dredge level

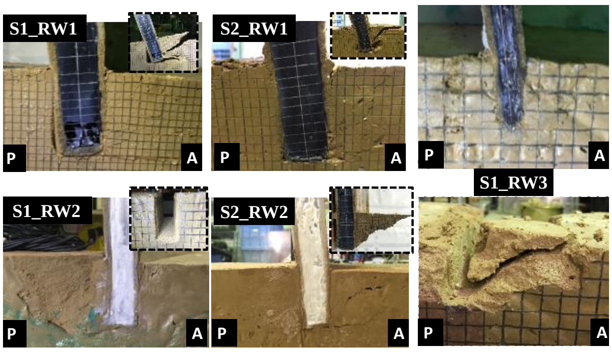

Fig. 11 Observed deformation and failure of walls

medium that can be seen even at 95g centrifugal acceleration. It can be confirmed by means of physical evidence provided in **Fig. 11**. Overall from the observations, it can be concluded that, the wall with 3 m embedment in sand rock (S1_RW2) could maintain the stability even under large horizontal and moment loads. However, for the application of self-standing walls in mud rock, the stability of wall with increased embedment depths (d_e > 3 m) must be confirmed.

Measured earth pressures in the front and back side of the embedded portion of the wall are plotted against the wall top displacements in **Fig. 12** and **Fig. 13** respectively. Observed pivot points from digital images of deformed wall at the end of loading process are provided in parenthesis. From **Fig. 13**, a clear decreasing trend of earth pressures can be observed in the initial stages of wall movement. This observation reveals the gradual loss of contact between the earth pressure cell and the embedment medium. Also, the observed loss of pressure at the back side and the increase in front (S1_RW1, S2_RW2) at relatively small wall top displacements could be attributed to the lateral translation of the wall. It is important to note that the soft rocks used in this study are relatively stiff and self-standing height of model soft rocks are much higher than the embedment depths. Also, the wall in S1_RW2 does not show a clear response during the entire loading process.

Mobilization of passive pressures with wall top displacements for the walls in S1_RW1, S1_RW3 and S2_RW1 can be observed **Fig. 12**. As the wall move and rotate towards the front as depicted in **Fig. 14**, passive resistance induced by the embedded medium also increases with the wall movement. This observation is as expected since the earth pressure cells are located above the point of rotation. However, a clear mobilization cannot be seen for the wall in S2_RW2. The possible reason for this observation could be the relatively deeper location of the earth pressure cell in front compared to the point of rotation. This argument could be supported by referring to the observed rise of passive pressure at relatively large wall top displacements at the back side of the wall in S2_RW2. Over all from the observed pressure variations in front and back side with the wall movement, it can be concluded that the net earth pressure profile is a combination of passive pressure zones in front and back side of embedded length of the wall. Also, the active and passive earth pressure zones can be switched based on the point of rotation. **Fig. 14,** shows a typical failure mode observed for a self- standing wall (S2_RW1) embedded in

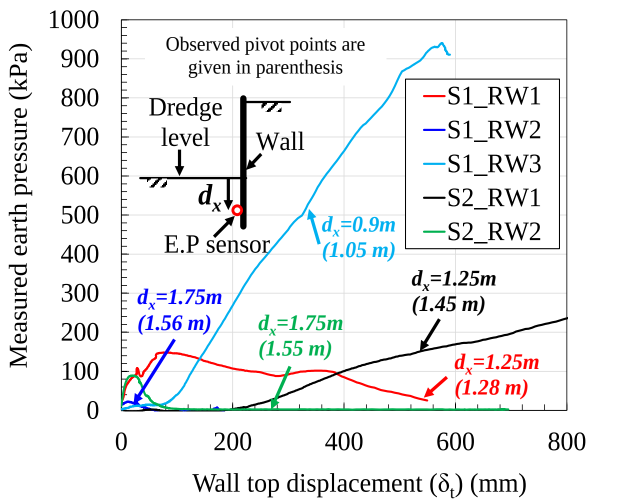

Fig. 12 Change of measured earth pressures in the wall front embedded portion against the wall top displacement

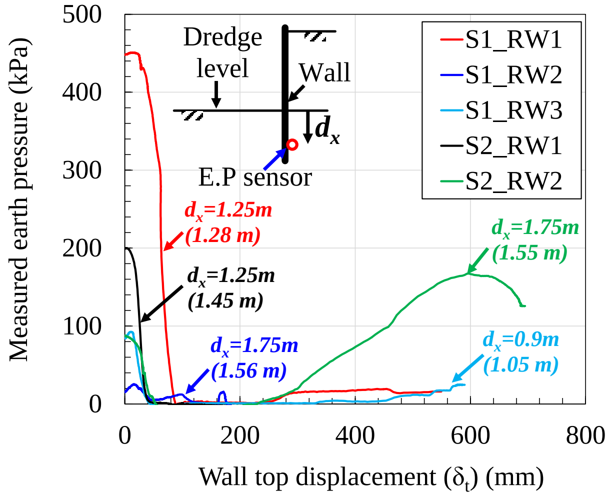

Fig. 13 Change of measured earth pressures in embedded portion at the back side of the wall against wall top displacement

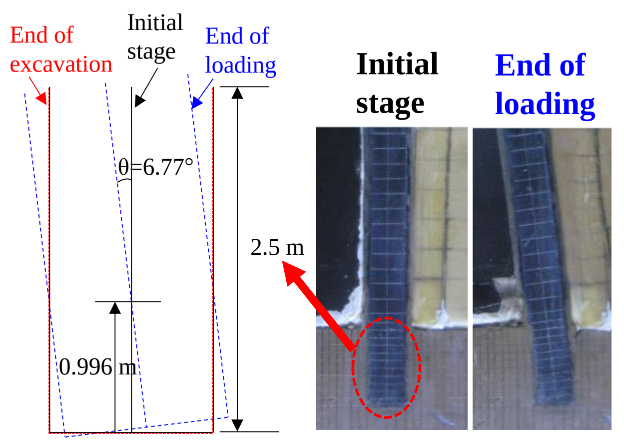

Fig. 14 Typical failure pattern observed for wall"R" in S2_RW1 and the deformation profile in the embedment zone

soft rock with a relatively small embedment depth. From depicted deformation profile in the embedded zone, a translation and rigid body rotation modes of deformations could be observable at the end of excavation and at the end of loading respectively. Based on the observed failure modes and the earth pressure mobilizations as described in **Fig. 12** and **Fig. 13**, an idealized pressure distribution was drawn for the stability analysis as shown in **Fig. 15**.

Referring to the observed failure mode in **Fig. 14**, certain amount of base shear as well as side wall frictions could be expected in the embedded zone as a favorable action against the failure of the wall. However, the contribution of above mentioned forces is not considered in this stability analysis. This assumption could underestimate the factor of safety (*FOS*) and yield a stable condition of wall even below the *FOS* equals to unity. The factor of safety against the rotational failure about the pivot point which is located at a depth d_o from the dredge level can be written as a ratio between resisting moments (M_R) and driving moments (M_D). The *FOS* (M_R/M_D) can be derived from the pressure distributions described in **Fig. 15**, where γ_d and γ_R are unit weight of backfill sand (γ_d=15.6 kN/m^3) and soft rock (γ_R=20.1 kN/m^3) respectively. Also, K_a is the active earth pressure coefficient of sand and C_u represents the undrained shear strength of soft rock.

A stability analysis was conducted on a self-standing wall embedded in soft rock with undrained shear strength of 650kPa and fixed retain height of 12 m. In this analysis, the critical depth of the pivot point was estimated using the principle of minimization of moment ratio as described by Madabushi, et al. (2005). For different embedment depths, *FOS* against rotational failure was estimated by varying the loading height of water in the back side of the wall. Based on the estimated *FOS* and the corresponding loading height of water, the imposed moment loads (M_L) at the dredge level was estimated. Graphical representation of estimated moment loads against the embedment depths at different *FOS* are presented in **Fig. 16**.

Assumed strength of the embedded medium (C_u=650kPa) and wall dimensions (H, d_e) in this analysis are identical to the condition of S1_RW1 and S1_RW2 which are 2.5 m and 3 m embedment in sand rock. **Fig. 17**. shows the experimental observations for the walls

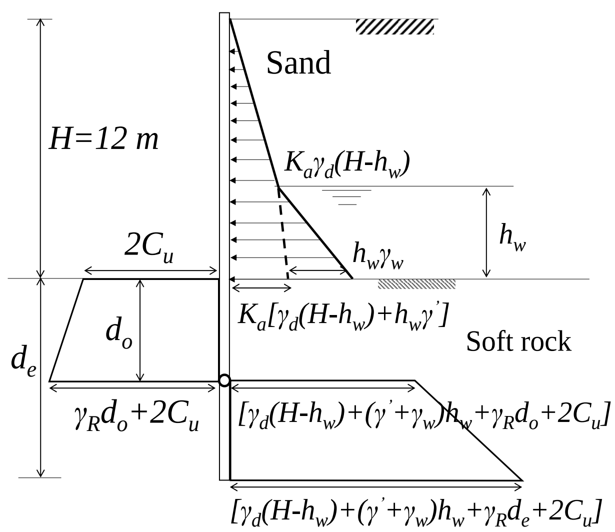

Fig. 15 Assumed earth pressure profile for stability analysis

embedded in sand and mud rocks, in which applied moment loads against the embedment depth at different stages of wall top displacement (δ_t/H) are plotted **Fig. 17**. Increasing wall top displacements can replicate the decrease of *FOS*. Considering the theoretical and experimental observations for 2.5 m and 3 m embedment in sand rock and mud rock, a clear agreement can be seen in the trend of increasing moment load. Larger the wall top displacements are, the higher the stiffness ($\Delta M_L/\Delta d_e$) between the moment load observed for 2.5 m and 3m embedment depths become, which can be observable with the decrease of *FOS* in the theoretical analysis. However, the observed moment load (M_L) for mud rocks in **Fig. 17** exhibits no further increase from δ_t/H =1% to 2% which clearly indicates that the wall with 3m embedment in

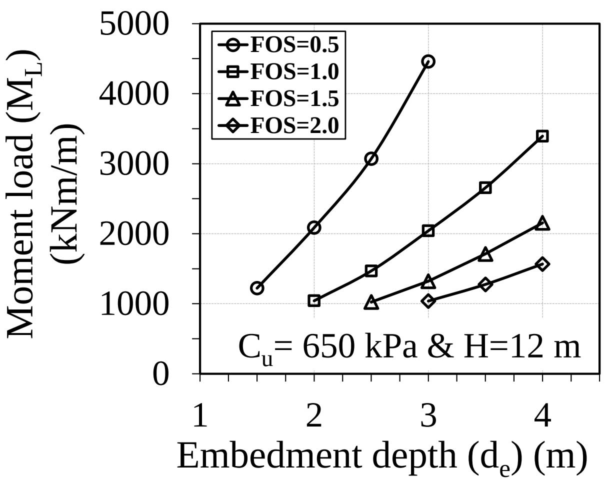

Fig. 16 Variation of moment load at dredge level against the embedment depth for different FOS based on stability analysis

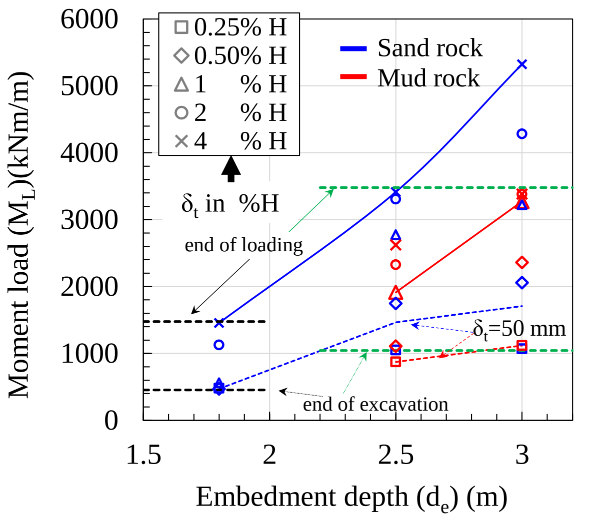

Fig. 17 Influence of embedment depth on the stability of self-standing walls embedded in soft rocks

in mud rock reached its ultimate capacity around 120 mm wall top displacements.

Considering 2% (50mm=0.4%*H*) and 10% (250mm=2%*H*) of the pile diameter as allowable and ultimate limits of the wall top displacements, it can be said that the 2.5 and 3 m embedment depths in sand rock can secure the allowable displacements under design loads (end of excavation) with a reasonable safety margin. Considering the stability of walls in mud rock, the 3 m embedment depth is not adequate to provide an additional safety margin over the allowable limit, therefore further increment of embedment depth is necessary to control the wall deformations within allowable limits with an additional factor of safety. From **Fig. 17** it can be confirmed that the wall in S1_RW2 could sustain large lateral loads even after the ultimate limits of deformations (2%*H*). This observation clearly indicates that the wall with 3 m embedment in sand rock could maintain the stability even at ultimate loading conditions with a reasonable safety margin. Also, an 0.5 m increase of embedment in sand rock significantly improved the stability and failure behavior of wall under design and ultimate loading conditions.

4. Conclusions

Stability of walls embedded in soft sand rocks can be secured with a relatively smaller embedment depth than that of current design practices. However, the behavior in mud rocks must be well studied with an increased embedment (de >3 m) depth to secure the stability under ultimate loads.

A small increment (0.5 m) in the embedment depth significantly increased the stability and failure loads of self-standing walls embedded in soft rocks.

Failure of self-standing walls embedded in soft rocks take place by rigid body rotation about the pivot point which is located far above from the bottom tip of the wall.

References

Association of Steel Pile. 2009. Design manual of self-standing steel sheet pile wall.

Gopal Madabhushi, S.P. and Chandrasekaran, V.S. 2005. Rotation of cantilever sheet pile walls. Journal of geotechnical and geoenvironmental engineering, 131 (2), pp. 202-212.

Johnston, I.W. and Chiu, H.K. 1984. Strength of weathered Melbourne mudstone. Journal of Geotechnical Engineering, 110 (7), pp. 875-898.

Kunasegaram, V., Seki, S., Takemura, J. 2015. “Modeling of soft rock for a centrifuge study”, Proc. 12th GeoKanto, pp. 15-19.

Kunasegaram, V., Seki, S., Takemura, J. 2018, “Deflection and failure of self-standing high stiffness steel pipe sheet pile walls embedded in soft rocks”, Proc. 9th ICPMG, pp. 1439-1444.

Lo, Kwan,Y., Micic, S., Lardner, T. and Janes, M. 2009. Geotechnical properties of a weak mudstone in downtown Calgary. GeoHalifax’09.

Takemura, J., Kondoh, M., Esaki, T., Kouda, M. and Kusakabe, O. 1999. Centrifuge model tests on double propped wall excavation in soft clay. Soils and Foundations, 39 (3), pp. 75-87.